International Journal of GEOMATE, Oct. 2023, Vol. 25, Issue 110, pp.87-97
ISSN: 2186-2982 (P), 2186-2990 (O), Japan, DOI: https://doi.org/10.21660/2023.110.3959
Geotechnique, Construction Materials and Environment

# ANALYZING RECENT SEISMIC ACTIVITY OF THE OPAK FAULT SYSTEM IN CENTRAL JAVA, INDONESIA, FROM 2009 TO 2021

*Ayu Krisno Ekarsti[13], Subagyo Pramumijoyo[2], Gayatri Indah Marliyani[2], Agung Setianto[2], and Dwikorita Karnawati[23]

[1]Doctoral Program in Geological Engineering, Faculty of Engineering, Universitas Gadjah Mada, Yogyakarta, Indonesia; [2]Departement of Geological Engineering, Faculty of Engineering, Universitas Gadjah Mada, Yogyakarta, Indonesia; [3]Agency for Meteorology Climatology and Geophysics (BMKG), Jakarta, Indonesia

*Corresponding Author, Received: 31 May 2023, Revised: 27 July 2023, Accepted: 3 Aug. 2023

**ABSTRACT:** A strong earthquake occurred on May 26, 2006, at 22:53:58 UTC, with a magnitude of Mw6.4. The shock was felt with an intensity of VI-VII MMI around Yogyakarta, Indonesia. The earthquake was presumably caused by the movement of the Opak Fault. Following the strong earthquake, seismic activity along the fault has remained high to this day. In order to explain the progression of seismic activity and understand the mechanism of the Opak fault, we conducted catalog relocation, focal mechanism inversion, and statistical analysis of the earthquake events from 2009-2021. The events were relocated using the Double Difference Method. To improve the accuracy of the focal mechanism inversion, we updated the 1-D velocity model from Crust 1.0 to a local velocity model. We inverted the mechanism of earthquakes with a magnitude of M≥3.0. The results indicate that the recent hypocenters are clustered in the southeastern part of the Opak Fault. This cluster is located within the rupture zone of the Mw6.4 2006 mainshock, providing further evidence that post-earthquake deformation from 2006 is still ongoing and primarily involves left-lateral oblique-slip faulting. The mechanism results are consistent with the observable morphological contrast on the surface. Cross-section plots of seismicity and dip angle, perpendicular to the mainshock strike, reveal a flower structure pattern, indicating a complex mechanism. The fault system is believed to be in the interseismic period, supported by the low b-value. The suspicion is further strengthened by an increase in microseismic activity and a decrease in M>3.0. This evidence suggests that the Opak Fault is currently experiencing strain accumulation.

*Keywords: Opak fault, Double difference, Couple velocity hypocenter, Focal mechanism, Flower structure*

## 1. INTRODUCTION

The tectonic region of Yogyakarta is primarily influenced by an active Sunda subduction zone. The convergence between the Indo-Australian Plate and the Eurasian Plate in this subduction zone has resulted in the presence of active faults, including the Opak Fault system, as well as a mountain complex that consists of Mt. Merapi, Mt. Merbabu, and Mt. Telomoyo located to the north of Yogyakarta [1,2]. On 27 May 2006, a strong earthquake associated with the activity of the Opak Fault occurred, measuring a magnitude of Mw6.4 and reaching a maximum intensity of VI-VII MMI [3]. This earthquake caused 6.324 fatalities, 36.299 injuries, and damage to 616.458 buildings [4]. The historical record of destructive earthquakes (Fig. 1(a)) indicates that shallow crustal earthquakes have caused significant damage. It has been documented that at least three destructive earthquakes have occurred along the Opak fault, suggesting that it has the potential to generate future destructive earthquakes. The presence of densely populated settlements and urban areas surrounding the fault increases the level of earthquake disaster risk.

The position, dimensions, segments, and mechanism of the fault remain subject to debate among researchers. The Opak Fault's position has been depicted primarily along the Opak River [2], but the localization of the mainshock and aftershock distribution, as indicated by [5] and [6], does not align exactly with [2]. Instead, it clusters in a parallel manner and shifts towards the southeastern direction. Validation of these findings could be accomplished by identifying surface ruptures in the field. However, after the 2006 Yogyakarta earthquake, a field identification conducted by [7] found no surface rupture around the Opak Fault. Some researchers propose that the fault structure responsible for the 2006 mainshock is located east of the Opak River [6,8-11]. According to temporal geodetic observation conducted by [12], the fault mechanism is primarily dip-slip. There is also suspicion of the existence of other faults with a sinistral strike-slip mechanism in the southern part.

According to reports from [13] and [14], the seismic activity along the Opak Fault remains high to this day. Accurate determination of the hypocenter and earthquake source parameters is

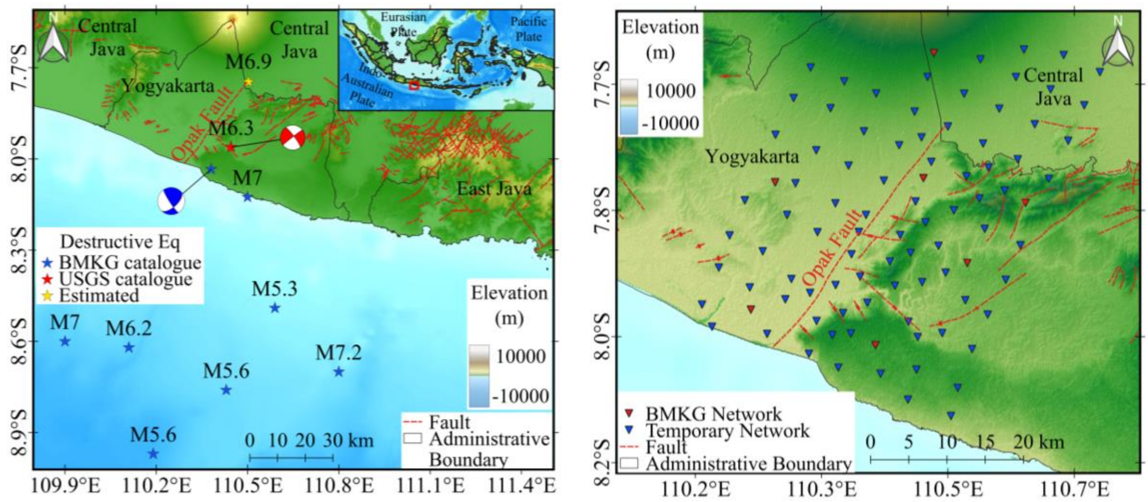


(a) (b)

Fig.1 (a) The map displays the historical record of destructive earthquakes in Yogyakarta. The earthquake focal mechanisms are depicted using beachball plots [1] and [2]. The insert map showcases the Indonesian region, along with the Indo-Australian plate motions relative to the Eurasian plate. The study area is marked by a red rectangle. (b) The map illustrates the BMKG seismic network and the temporary seismic array network. The topography is represented using DEM data [16]. The red dashed lines indicate the faults, both active and inactive, in the vicinity of Yogyakarta, adapted from [1] and [2]. The black line indicates the provincial administrative boundary, adapted from [17] and [18].

crucial in order to understand the origin of an earthquake. These parameters are necessary for identifying the characteristics of active faults. The objective of this study is to characterize the recent behavior of the Opak Fault by utilizing the results of hypocenter relocation, focal mechanism inversion, and statistical analysis. The findings from this study can be utilized to update earthquake hazard maps in Yogyakarta.

## 2. RESEARCH SIGNIFICANCE

In this study, we conducted a detailed investigation into the current development of seismic activity along the Opak Fault. The brittle zone was identified based on the clustered earthquake position obtained through relocation. By performing statistical analysis, we were able to analyze the spatial and temporal seismicity and temporal moment release trends. Additionally, the statistical analysis allowed us to determine the b-value, which is indicative of the stress level within the fault system.

Furthermore, we updated the local velocity model specific to the Opak fault system. This refined local velocity model enables more accurate computation of the Green Function and calculation of kinematic parameters. The focal mechanism model derived from this research provides insights into the fault system's mechanism. Examining the earthquake clusters alongside the focal mechanism helps determine whether the current seismic activity is still associated with the 2006 Mw6.4 earthquake or represents independent activity. Moreover, the clusters and focal mechanisms contribute to understanding the morphological characteristics around the Opak Fault. The findings of this research add to the existing knowledge and enhance our understanding of the Opak Fault system.

## 3. METHODS

The earthquake data utilized in this study is divided into three distinct periods. The first period spans from January 1, 2009, to September 1, 2021. The second period covers the timeframe of September 2 to December 8, 2021. Finally, the third period ranges from December 9 to December 31, 2021.

For the first and third periods, we employ earthquake parameter data along with the arrival times of P-waves and S-waves acquired from the BMKG catalog as documented in references [13] and [14]. However, during the second period, we supplemented the existing BMKG network with 86 temporary arrays. These temporary arrays are strategically installed to enhance the detection and characterization of micro-earthquake events. The configuration of the temporary station's arrays is set at a distance of 5 km to ensure detailed analysis. A distribution map illustrating the utilized seismic network is presented in Figure 1(b).

### 3.1 Temporary Network Specification and Preparation

The BMKG seismic network consists of

broadband seismographs. We supplement the BMKG seismic network with the portable seismic network that consists of 12 portable broadband seismographs and 11 portable short-period seismographs. Portable broadband seismographs are installed stationary at the edges and the middle of the study area. Portable short-period seismographs are installed mobile, with an operation time of about 15 days per point. A portable broadband seismograph consists of a Trillium Compact Posthole seismometer 0.008-100 Hz and a Pegasus Digital Recorder digitizer. A portable short-period seismograph consists of Lennartz LE-3Dlite MkIII seismometer 1-100 Hz and a Taurus digitier. Both pieces of equipment are operated on three channels with a sampling frequency of 100 Hz. There is no significant difference in the use of broadband or short-period seismographs because the target of deployment is the detection of micro-seismic activity that dominantly happened over a short period.

Before the seismographs were utilized, We did the recording intercomparison as a calibration. All seismographs were installed in the same location. Then, seismographs were operated simultaneously for 30 minutes. The duration was enough to record the seismic wave up to the minimum frequency of 0.2 Hz [15]. This minimum frequency is more than sufficient to detect microearthquake activity. We make sure all seismographs always have the same recording response. When We found a record that was different from other responses, the abnormality might occur in the seismometer or the recorder. Of course, We did not use the seismograph that has the abnormality.

### 3.2 Detection and Hypocenter Localization

Earthquake detection employed the characteristic function using the Lassie package [19] from the Pyrocko library [20] of the Python program. The waveform data underwent normalization, smoothing, and stacking processes to generate characteristic functions. A detection threshold was then set. The estimated origin time was determined as the point when the characteristic function value surpassed the threshold value. Once the detection was completed, we obtained the estimated origin time, and location of the earthquake events.

Subsequently, we utilized the detection results to manually pick the arrival times of P and S waves using the Seiscomp software package [21]. The earthquake parameters, including latitude, longitude, depth, origin time, and magnitude, were calculated using the hypo71 plugins within Seiscomp [22]. To compute the earthquake position and origin time, we employed the Wagner velocity model [23] (as presented in Table 1).

### 3.3 Hypocenter Relocation

We utilized P-wave and S-wave arrival time data compiled from 2009 to December 2021 for our analysis. These events were relocated using the Double Difference method [24] implemented through the HypoDD program [25]. The method operates on the assumption that if there are two earthquakes located closer to each other than the distance from their respective hypocenters to the station, their ray paths and the medium can be considered equal.

For this study, we set the maximum distance (MAXSEP) between earthquakes to be considered as having the same path as 15 km. The maximum distance between earthquake pairs and stations (MAXDIST) was set at 500 km. Additionally, we limited the maximum number of earthquakes considered to form a group (MAXNGH) to 20 earthquakes. Through iterative updates, the earthquake kinematic parameters and residual values for each parameter were refined. The parameters resulting from the final relocation were obtained from the last iteration. In our analysis, we also utilized Wagner's 1-D velocity model to relocate the hypocentres.

Table 1 1-D Velocity model [23]

| Depth (Km) | Vp (Km/s) | Vs (Km/s) |
|---|---|---|
| 0 | 4.3 | 2.4 |
| 3 | 4.9 | 2.9 |
| 8 | 5.7 | 3.2 |
| 16 | 6.9 | 3.9 |
| 24 | 7.1 | 4 |

### 3.4 Statistics Analysis

The relocation results were specifically focused on earthquake events occurring in the vicinity of the Opak Fault. To assess the seismicity, we applied the Guttenberg-Richter rule, plotting the cumulative magnitude against the number of earthquake events [26]. The magnitude of completeness was determined from this plot using the Maximum Likelihood method [27]. This analysis was conducted using the Zmap software [28]. By obtaining the magnitude of completeness, we can evaluate the effectiveness of the seismic network in capturing seismic activity. To depict the cumulative rate of energy release along the Opak Fault, we plotted the temporal cumulative seismic moment. The seismic moment was derived by converting magnitudes using the Hanks and Kanamori formula [29]. By examining the cumulative energy rate, we can gain insights into the total energy released by the fault system during a specific period.

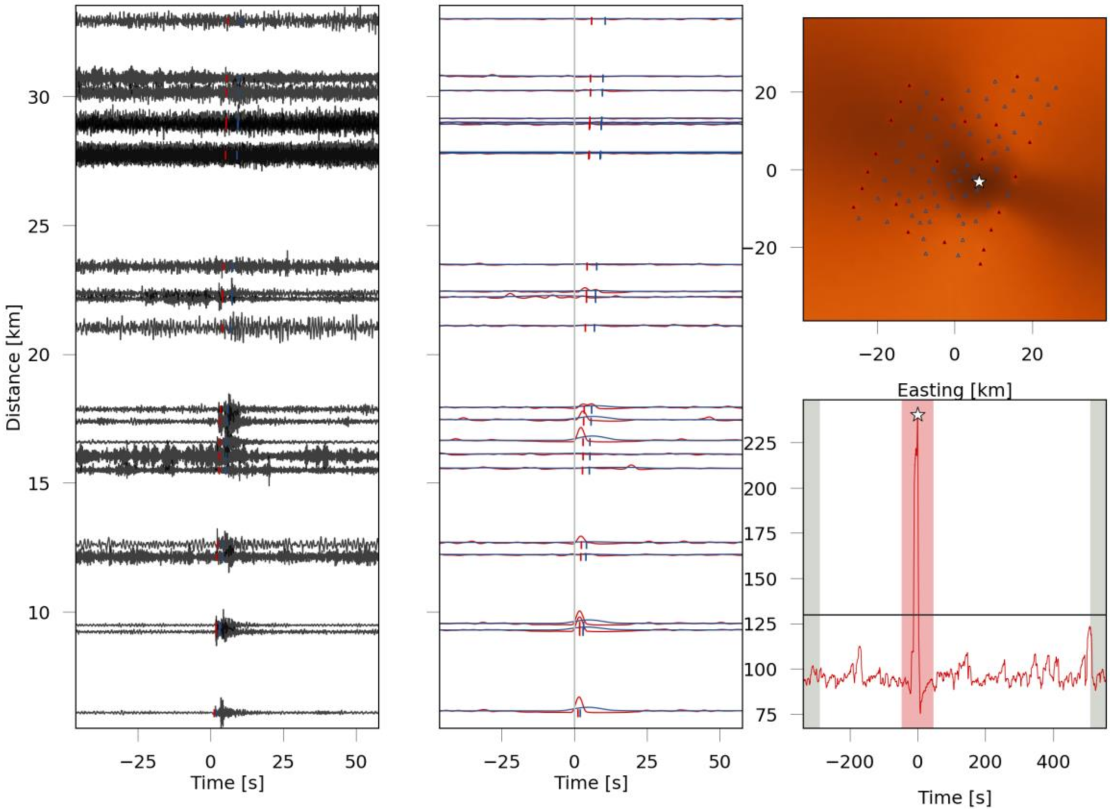


Fig.2 Example of microearthquake detection result for M1.1, September 23, 2021. We used a threshold of 130. The characteristic function is valued at 240. The left column shows the raw waveform. The middle column shows the normalized and smoothed waveform (characteristic function). The bottom right column shows the stacked characteristic function. Right upper shows the estimated microearthquake location.

### 3.5 Local Velocity Modeling

To ensure accurate calculations of the green function, we updated the 1-D velocity model. For the modeling, we employed the couple velocity hypocenter method. This method, similar to the Double-Difference method, utilizes non-linear inversion computation through a linear approach. However, the couple velocity hypocenter method simultaneously generates updated velocity models, kinematic parameters, and station corrections during the inversion process. The inversion was performed using the Velest [30,31]. The earthquake parameter and arrival time data used for hypocenter relocation were also utilized in this process. We utilized the Crust 2.0 velocity model [32] as the initial model for local velocity modeling. The Crust2.0 model details are provided in Table 2.

Table 2 1-D Velocity model [29]

| Depth (km) | Vp (km/s) | Vs (km/s) | Rho (g/cm$^3$) |
|---|---|---|---|
| 0 | 2.5 | 1.2 | 2.1 |
| 1 | 4.0 | 2.1 | 2.4 |
| 2.5 | 6.0 | 3.4 | 2.7 |
| 13.5 | 6.6 | 3.7 | 2.9 |
| 23.5 | 7.2 | 4.0 | 3.1 |

### 3.6 Focal Mechanism Analysis

The purpose of modeling the earthquake focal mechanism around the Opak Fault system is to gain a deeper understanding of the fault's mechanism through moment tensor analysis. For this analysis, we utilized high-quality earthquake seismograms recorded by at least six seismic stations. The ISOLA program [33] was employed for modeling the focal mechanism. In order to establish a reference, we utilized the mechanism determined by [5] for the mainshock of the Mw6.4 Yogyakarta earthquake that occurred on May 26, 2006.

Modeling was conducted on earthquakes with a magnitude greater or equal to Mw3.0. Prior to the inversion stage, each seismogram underwent data preprocessing. This involved instrument response deconvolution, cutting, and initial filtering. We applied a Bandpass filter with a corner frequency ranging from approximately 0.1 to 0.6 Hz. The specific corner frequency for each seismogram was determined through a trial and error process during the inversion, aiming to achieve the best fit between the calculated (synthetic) seismogram and the observed seismogram.

To generate the calculated seismogram, we utilized the Green Function and employed the

Discrete Wave Number method [34]. The Green Function represents the medium through which earthquake waves propagate from the earthquake source to the station. In generating the Green Function, we utilized the local velocity model specific to the Opak Fault region.

## 4. RESULT AND DISCUSSION

We successfully detected 62 earthquake events in the temporary network data from September 2 to December 8, 2021. After manual picking, earthquake parameter calculation, and relocation, we eliminated nine events that were located outside the Opak fault system. Consequently, we selected a total of 53 events for further analysis. The effectiveness of scanning earthquake events using the Lassie algorithm has been demonstrated. The BMKG network can detect earthquake activity on the Opak Fault up to M1.3. With the addition of a temporary seismic network, earthquake events can be detected up to M0.7. This shows a significant increase in network capability for detecting earthquakes. An example of the detection results for a microearthquake that occurred on September 23, 2021, at 21:00:47 UTC, with a depth of 9.8 km and a magnitude of Ml1.1, is shown in Fig. 2.

We relocated the hypocenters of 192 events around the Opak Fault out of the initial 229 events (Fig. 5.a). During the relocation process, 37 events were excluded based on parameterization (Fig. 5.b). The earthquakes around the Opak Fault in the period from 2009 to 2021 had depths ranging from 0.9 km to 22.4 km and magnitudes ranging from ML 0.7 to 4.8. The residual time histogram indicates a significant improvement in data quality after relocation (Fig. 3.b), with the majority of residual times approaching 0 [35], compared with the residual time before relocation (Fig. 3.a).

The Guttenberg-Richter curve illustrates the relationship between the magnitude distribution and the cumulative number of earthquakes in the Opak Fault (Fig. 4.a). From the plot, the magnitude of completeness (Mc) determined from the relocated data is M1.2. The relatively small Mc indicates that the seismic network consisting of BMKG and the temporary network can detect earthquakes up to M1.2 with reasonable confidence. Therefore, the network's ability to detect microearthquakes is quite good. The b value, obtained from the plot, is 0.3. The magnitude completeness and b value are lower than the calculation of [36] that was calculated using BMKG and combined with the global catalog. The obtained relatively low b value could be attributed to two possibilities. The first possibility is the increased network density resulting from the addition of four stations by BMKG in 2019 and the deployment of the temporary network in 2021. A denser seismic network leads to a higher number of recorded microearthquakes. The second possibility is a natural increase in microearthquake activity, suggesting that the Opak Fault may be accumulating stress [37]. The fact is that microseismic activity appears to have increased while the number of ML>3.0 events decreased (Fig. 4.b). The cumulative moment release (Fig. 4.c) indicates that from 2009 to 2021, the Opak Fault released an energy equivalent to Mw4.8, reaching a total of $2.31 \times 10^{16}$ Nm. This suggests that since 2009, there has been no significant energy release, and the Opak Fault may be in a period of quiescence. During this period, strain accumulates due to fault interlocking.

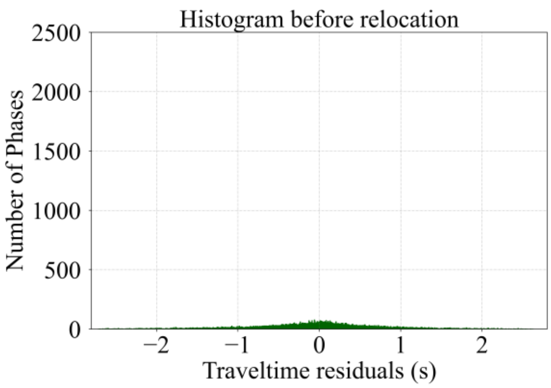


(a)

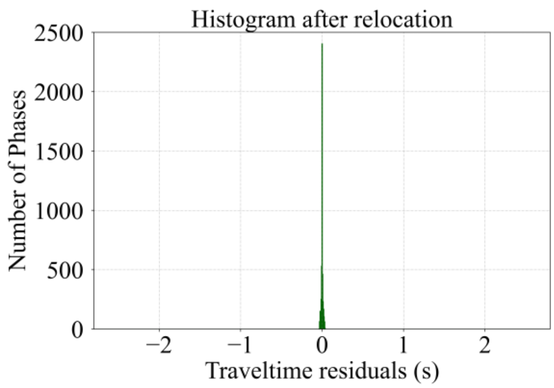


(b)

Fig.3 The travel time residual histogram (a) before relocation and (b) after relocation.

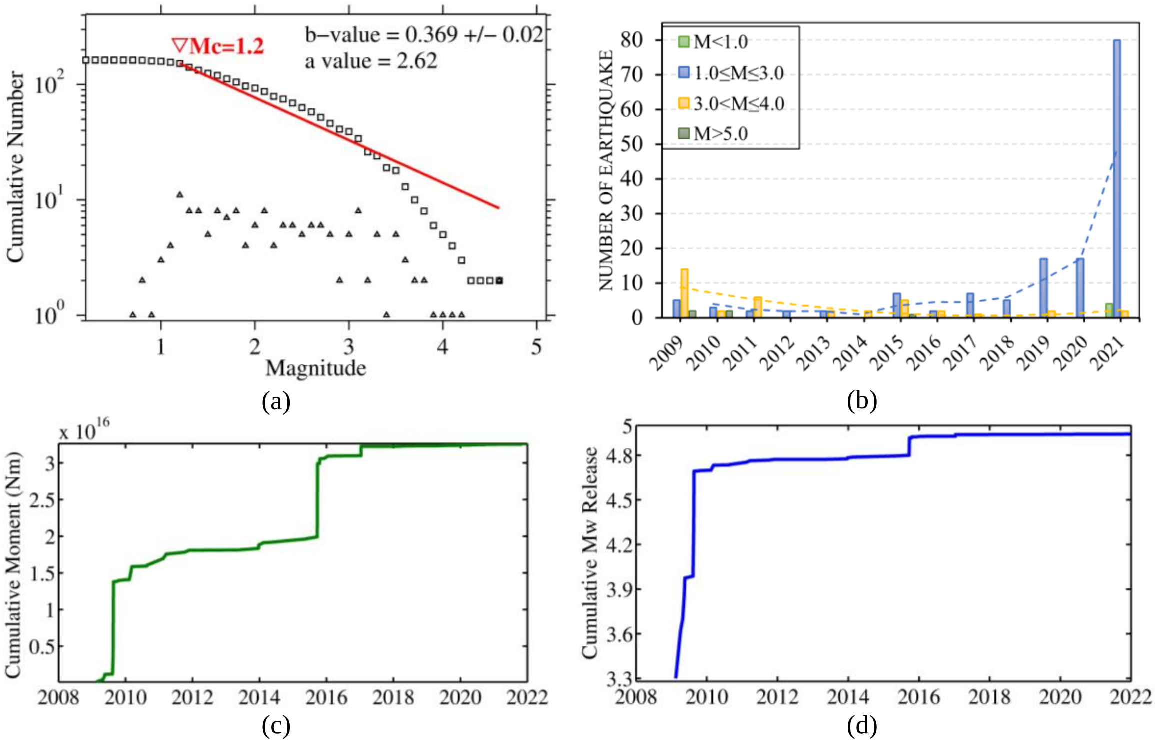


Fig.4 (a) The Guttenberg-Richter curve based on relocation data. (b) Seismicity Trend Around the Opak Fault 2009-2021. (c) The cumulative moment release (d) The cumulative moment in moment magnitude.

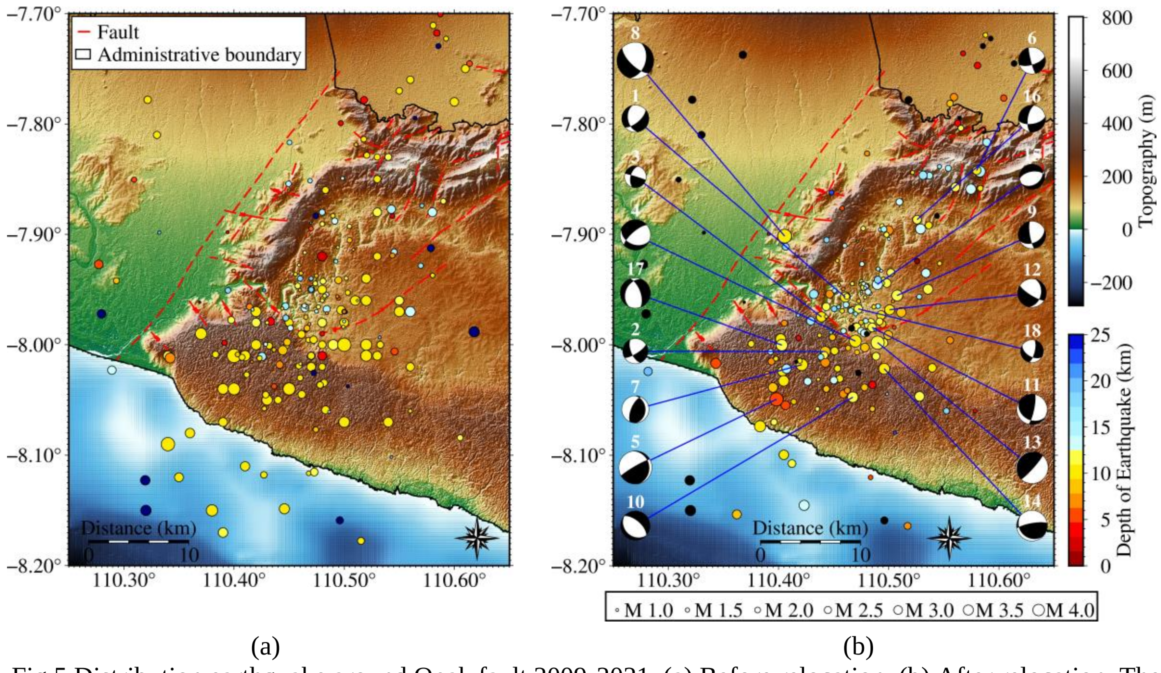


Fig.5 Distribution earthquake around Opak fault 2009-2021. (a) Before relocation. (b) After relocation. The beach ball shows the solution to the focus mechanism of earthquakes around the Opak Fault. The black dots show the events that excluded due to the parameterization. The red dash-line depicts the fault from [4] and [5]. The topography is represented using DEM data [16]. The black line indicates the provincial administrative boundary, adapted from [17] and [18].

The earthquake distribution map (Fig. 5) clearly shows that the relocated earthquake positions appear more lineated and less scattered compared to before relocation. The relocated data aligns with the southeastern part of the Opak Fault, consistent with the aftershock cluster position of the 2006 Yogyakarta earthquake analyzed by [38]. The relocated data is slightly to the east compared to the results of [38] and primarily clusters in the Southern Mountain escarpment.

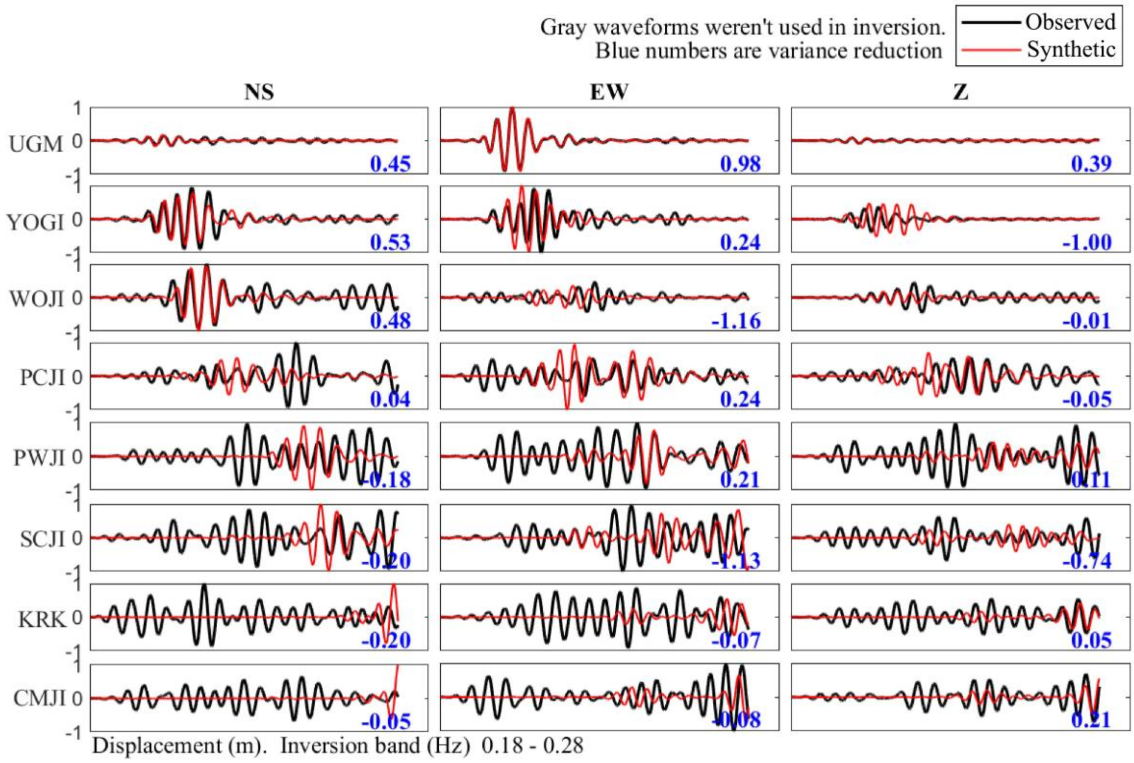


Fig.6 Example of waveform fitting obtained from waveform focal inversion for Mw3.6, March 21, 2011 earthquake. Station used are UGM, YOGI, WOJI, PCJI, PWJI, SCJI, KRK, and CMJI. The red curve denotes the synthetic waveform, and the black curve denotes the observed waveform.

These locations also correspond to the positive stress coulomb zone of the 2006 earthquake [40]. Therefore, the recent earthquake activity is believed to still occur in the same zone as the 2006 Yogyakarta earthquake. These findings support the hypothesis that post-earthquake deformation from the 2006 earthquake is still ongoing.

The updated velocity model is presented in Table 3. Overall, the updated model shows higher values compared to the initial model, except for the Vs values at a depth of 0 km and 2.5 km.

Table 3 1-D Velocity model

| Depth (km) | Vp (km/s) | Vs (km/s) |
|---|---|---|
| 0 | 4.49 | 0.48 |
| 1 | 4.49 | 2.9 |
| 2.5 | 4.82 | 3.05 |
| 13.5 | 7.42 | 4.31 |
| 23.5 | 7.77 | 4.31 |

Focal mechanism inversions were performed for 18 events with magnitudes greater than M3.0. The quality of the inversions was assessed by examining the fit between the synthetic and observed seismograms. An example of the seismogram fitting for the Mw3.6 earthquake on March 21, 2011, is shown in Fig. 6. The complete inversion results are displayed as beachball plots in Fig. 5.b. The results indicate that the mechanisms of the Opak fault are quite diverse but are predominantly characterized by left-lateral oblique-slip faults. The southern part of the fault is dominated by a thrust fault, which is located in the southern mountain zone. According to [40,41], continental plates collided in the Cretaceous period beneath the southern mountain zone. This collision may be related to the reverse fault mechanism observed in the southern part.

To identify the vertical distribution of the hypocenters, cross-sections perpendicular to the selected focal mechanism strikes were created. The cross-section positions are shown in Fig. 7a. Cross-sections FM1-FM1' (Fig. 7.b), FM2-FM2' (Fig. 7.c), FM3-FM3' (Fig. 7.d), and FM4-FM4' (Fig. 7.e) are perpendicular to the strikes of the Mw3.4 event on May 13, 2009, the Mw6.4 event on May 26, 2006, the Mw3.6 event on April 30, 2016, and the Mw3.6 event on October 2, 2009, respectively.

The cross-sections reveal that the selected earthquakes dip to the east. On the cross-section plots, dashed lines with slopes equal to the dip angles for the earthquakes with focal mechanisms are added. These lines delineate the positions where surface manifestations could potentially occur. However, it is important to note that not all earthquakes can generate surface manifestations. The green triangles indicate the projected positions on the surface.

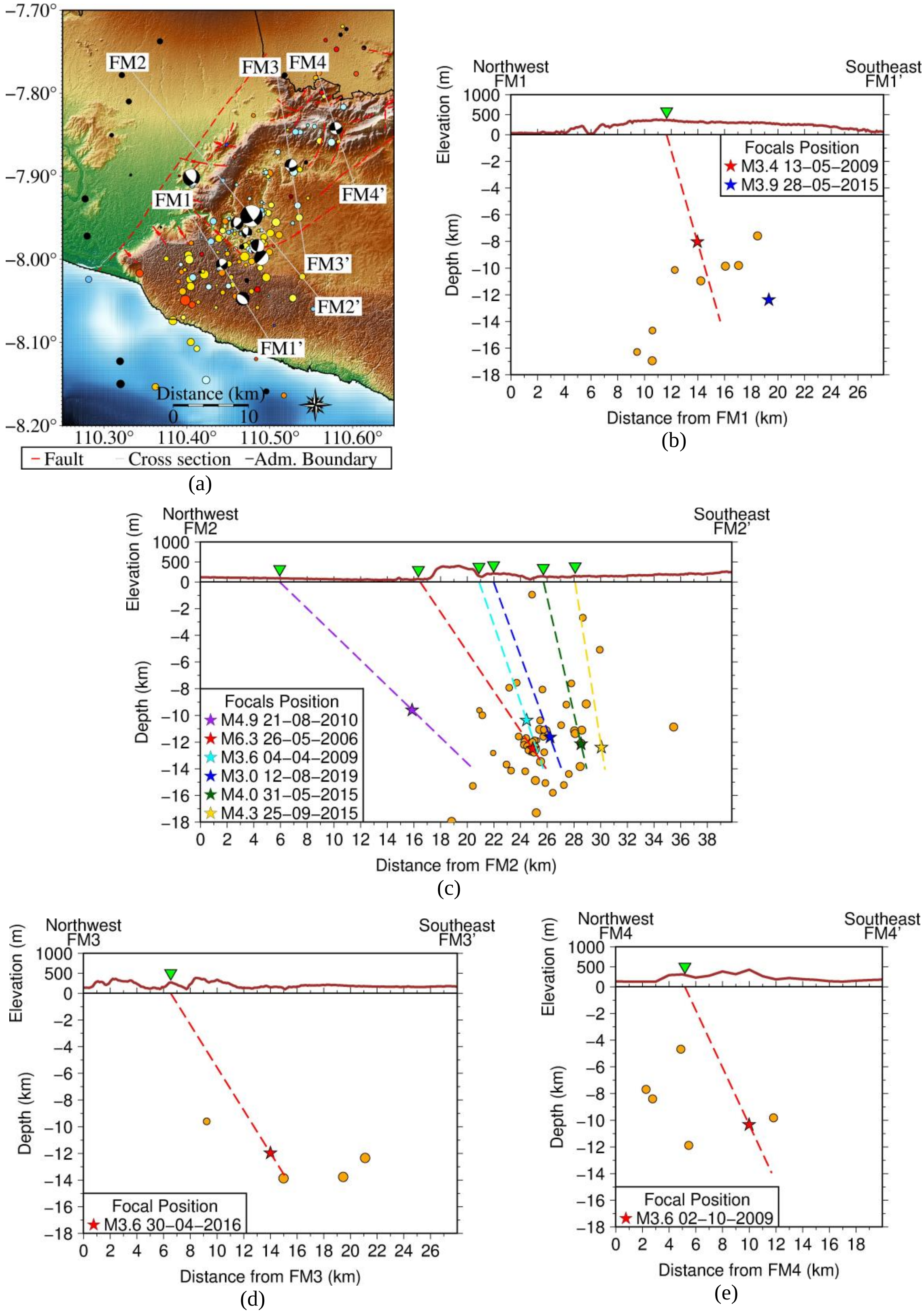


Fig.7 (a) The hypocenter cross sections perpendicular to the selected strike of the focal mechanism. (b) Cross-sections FM1-FM1', (c) FM2-FM2', (d) FM3-FM3', and (e) FM4-FM4'. The dashed lines represent the projected dip of the earthquake with the focal mechanism on the sections. The stars represent the hypocenter of focal mechanisms. The orange squares represent the hypocenter. The green triangles represent the projected earthquake with focal mechanisms by dip angle on the surface. The topography is represented using DEM data [16]. The black line indicates the administrative boundary, adapted from [17] and [18].

Fig. 7b-e illustrates that the green triangles correspond to morphological contrasts on the surface. Only a few hypocenters are captured by the FM1-FM1', FM3-FM3', and FM4-FM4' sections, while the FM2-FM2' section captures more hypocenters than the others. The mechanisms observed in the FM2-FM2' section are primarily left-lateral strike-slip. Most hypocenters follow the dipping trend of the focal mechanisms in this section. Based on the dipping and the hypocenter trend, the faulting pattern resembles a flower structure. A flower structure is a geometry that resembles a flower, where fault segments bloom at the top and accumulate at the bottom. This structure is formed in the wrench zone of a strike-slip fault [42]. This finding may explain the existence of the Wonosari depression zone. The Wonosari depression exhibits low topography around the earthquake cluster (Fig. 5 and Fig. 7). The depression zone around the wrench zone of the strike-slip fault confirms that the type of flower structure observed is a negative flower structure [42]. Consequently, the Wonosari depression could be formed by the flower structure beneath it.

## 5. CONCLUSION

The recent seismic activity on the Opak fault is clustered in the southeast, consistent with the location described by [6]. This recent cluster falls within the same zone as the Mw6.4 earthquake in 2006. The dominant mechanism of the recent earthquakes is characterized by a left-lateral oblique-slip fault, indicating a complex faulting mechanism. Some mechanisms align with morphological contrasts observed on the surface. In the middle part of the fault, the earthquake mechanism is primarily left-lateral strike-slip, forming a negative flower structure. The presence of the Wonosari depression may be attributed to this flower structure. The temporal moment release suggests the potential for strain accumulation along the fault. It is important to note the possibility of a strong earthquake, considering the historical seismicity and the current state of moment release.

However, the subsurface conditions associated with the unique seismicity trend and faulting complexity have not been thoroughly described in this study. Therefore, further investigation, using local tomography, for example, is necessary to provide a detailed understanding of the subsurface conditions within the Opak Fault system. Through subsurface modeling, the dimensions, the detailed dipping angle, and the blind segments of the Opak fault can be identified more accurately. The identification of blind segments adds validation to current seismic and morphological lineament trends. Furthermore, the identification can reveal the quiescence segments to be the next earthquake sources.

## 6. ACKNOWLEDGEMENTS

The author expresses gratitude to the Sleman Geophysics Station of BMKG for their valuable support and assistance throughout this research. Additionally, the author would like to extend thanks to the Education and Training Center of BMKG for providing the scholarship, the Earthquake and Tsunami Center of BMKG for their support in field equipment, and the Research and Development Center of BMKG for their funding support.

## 7. REFERENCES

[1] Surono, Toha B., and Sudarno I., Geological Map of the Surakarta–Giritontro Sheet, Jawa, Scale 1:100.000, Geological Research and Development Center, Bandung, 1992. (in Indonesian)

[2] Rahardjo W., Sukandarrumidi, and Rosidi H.M.D., Geological Map of the Yogyakarta Sheet, Jawa, Scale 1:100.000, Geological Research and Development Center, Bandung, 1995. (in Indonesian)

[3] Setiyono U., Gunawan I., Priyobudi, Yatimantoro T., Imananta R.T., Ramdhan M., Hidayanti, Anggraini S., Rahayu R.H., Hawati P., Yogaswara D.S., JuIius A.M., Apriani M., Harvan M., Simangunsong G., and Kriswinarso T., The Significant and Destructive Earthquake Catalogue of 1821 – 2018, Agency for Meteorology Climatology and Geophysics, Jakarta, 2019, pp.1-280. (in Indonesian)

[4] Irsyam M., Widiyantoro S., Natawidjaja D.H., Meilano I., Rudyanto A., Hidayati S., Triyoso W., Hanifa N., Djarwadi D., and Faizal L., Earthquake Source and Hazard Maps of Indonesia 2017. National Center for Earthquake Studies (PusGen), Research Center for Housing and Human Settlement, Directorate General for Research and Development, Ministry oof Public Works and People Housing, Bandung, 2017, pp.1-376. (in Indonesian)

[5] USGS, M6.3 - 10 km E of Pundong, Indonesia, https://earthquake.usgs.gov/earthquakes/eventpage/usp000ej1c/moment-tensor.

[6] Walter T.R., Wang R., Luehr B.-G., Wassermann J., Behr Y., Parolai S., Anggraini

A., Günther E., Sobiesiak M., Grosser H., Wetzel H.-U., Milkereit C., Brotopuspito P.J.K.S., Harjadi P., and Zschau J., The 26 May 2006 magnitude 6.4 Yogyakarta earthquake south of Mt. Merapi volcano: Did lahar deposits amplify ground shaking and thus lead to the disaster?, Geochemistry Geophysics Geosystem, Vol. 9, Issue 5, 2008, pp.1-9.

[7] Pramumijoyo S. and Sudarno I., Surface Cracking Due to Yogyakarta Earthquake 2006, The Yogyakarta Earthquake of May 27, 2006, Karnawati D., Pramumijoyo S., Anderson R. and Husein S., Ed., Star Publisher, Los Angeles, 2008, pp.6.1 – 6.5.

[8] Sadat D.I.K.F., Yudistira T., and Nugraha A.D., The Application of Ambient Noise Tomography Method at Opak River Fault Region Yogyakarta. AIP Conference Proceedings 18 July 2018 , Vol. 1987, Issue 1, 2018, pp.020028.1- 020028.7.

[9] Nurbaiti Y., Ibrahim E., Hasanah M.U., and Wijatmoko B., Application of Double-Difference Method for Relocating Aftershocks Hypocenters in Opak Fault Zone, IOP Conf. Series: Earth and Environmental Science, Vol. 311, Issues 2–4 July 2018, 2019, pp.1-6.

[10] Handayani L., Active Fault Zone of the 2006 Yogyakarta Earthquake Inferred from Tilt Derivative Analysis of Gravity Anomalies, RISET International Journal of Geology and Minning, Vol. 29, No. 01, 2019, pp.1-11.

[11] Saputra H., Wahyudi W., Suardi I., Anggraini A., and Suryanto W., The waveform inversion of mainshock and aftershock data of the 2006 M6.3 Yogyakarta earthquake, Geoscence Letters, Vol.8, No.9, 2021, pp.1-22.

[12] Widjajanti N., Pratama C., Parseno, Sunantyo T.A., Heliani L.S., Ma'ruf B., Atunggal D., Lestari D., Ulinnuha H., Pinasti A., and Ummi R.F., Present-Day Crustal Deformation Revealed Active Tectonics in Yogyakarta, Indonesia Inferred from GPS Observations, Geodesy and Geodynamics, Vol. 11, Issue 2, 2020, pp.135-142.

[13] Ikhsan, The Earthquake and Tsunami Annual Report of 2021, Agency for Meteorology Climatology and Geophysics, Yogyakarta, 2022, pp.1-239. (in Indonesian)

[14] BMKG, Earthquake Catalog, http://repogempa.bmkg.go.id/repo_new.

[15] SESAME, Guidelines for the Implementation of the H/V Spectral Ratio Technique on Ambient Vibrations: Measurements, Processing and Interpretation, SESAME European Research Project WP12, European Commission – Research General Directorate, 2004, pp.1-62.

[16] Geospatial Information Agency, National Seamless Digital Elevation Model (DEM) and Bathymetry (DEMNAS), https://tanahair.indonesia.go.id/demnas, 2018.

[17] National Coordinator for Survey and Mapping Agency, Topographical Map of Indonesia, Sheet 1407 of Pracimantoro, Scale 1:250.000, National Coordinator for Survey and Mapping Agency, Bogor, 2003. (in Indonesian)

[18] National Coordinator for Survey and Mapping Agency, Topographical Map of Indonesia, Sheet 1408 of Yogyakarta, Scale 1:250.000, National Coordinator for Survey and Mapping Agency, Bogor, 2003. (in Indonesian)

[19] López-Comino J. A., Cesca S., Heimann S., Grigoli F., Milkereit C., Dahm T., and Zang A., Characterization of Hydraulic Fractures Growth During the Äspö Hard Rock Laboratory Experiment (Sweden), Rock Mechanics and Rock Engineering, Vol. 50, No. 11, 2017, pp.2985–3001

[20] Heimann S., Kriegerowski M., Isken M., Cesca S., Daout S., Grigoli F., Juretzek C., Megies T., Nooshiri N., Steinberg A., Sudhaus H., Vasyura-Bathke H., Willey T., and Dahm T., Pyrocko - A Versatile Software Framework for Seismology, EGU General Assembly 2020, 2017.

[21] Helmholtz Centre Potsdam GFZ German Research Centre for Geosciences and gempa GmbH, The SeisComP seismological software package, GFZ Data Services, 2008.

[22] Lee W.H.K., and Lahr J.C., HYP071: A computer program for determining hypocenter, magnitude, and first motion pattern of local earthquakes, USGS, 1972.

[23] Wagner D., Koulakov I., Rabbel W., Luehr B.-G., Wittwer A., Kopp H., Bohm M., Asch G., and Scientists M., Joint inversion of active and passive seismic data in Central Java, Geophys.J. Int, Vol. 170, Issue 2, 2007, pp.923-932.

[24] Waldhauser F., and Ellsworth W.L., A double-difference earthquake location algorithm: Method and application to the

northern Hayward fault, Bull. Seism. Soc. Am., Vol. 90, No. 6, 2000, pp.1353-1368.
[25] Waldhauser F., HypoDD: A computer program to compute double-difference earthquake locations, USGS Open File Rep., 2001.
[26] Gutenberg B., and Richter C. F., Frequency of Earthquakes in California, Bulletin of the Seismological Society of America, Vol. 34, No.4, 1944, pp.185–188.
[27] Utsu T., A method for determining the value of "b" in a formula log n = a-bm showing the magnitude-frequency relation for earthquakes, Geophys. Bull. Hokkaido Univ., Vol. 13, 1965, pp.99–103.
[28] Wiemer S., A Software Package to Analyze Seismicity: ZMAP. Seismological Research Letters, Vol. 72, No. 3, 2001, pp.373-382.
[29] Hanks T. C., and Kanamori H., A Moment Magnitude Scale, Journal of Geophysical Research,Vol.84,IssueB5,1979,pp.2348-2350.
[30] Kissling E., Ellsworth W.L., Eberhart-Phillips D., and Kradolfer U., Initial reference models in local earthquake tomography, Journal of Geophysical Research: Solid Earth, Vol. 99, No. B10, 1994, pp.19635–19646.
[31] Kissling E., Program VELEST user's guide - short introduction, Institute of Geophysics, ETH Zurich, Zurich, 1995, pp.1-26.
[32] Bassin C., Laske G., and Masters G., The Current Limits of resolution for surface wave tomography in North America, Eos Transactions American Geophysical Union, Vol. 81, Issue F897, 2000.
[33] Sokos E.N., and Zahradník J., ISOLA a Fortran Code and a Matlab GUI to Perform Multiple-point Source Inversion of Seismic Data, Computers and Geosciences, Vol. 34, Issue 8, 2008, pp.967-977.
[34] Bouchon M., A Simple Method to Calculate Green's Functions for Elastic Layered Media, Bulletin of the Seismological Society of America, Vol. 71, No. 4, 1981, pp.959-971.
[35] Supendi P., Nugraha A.D., Puspito N.T., Widiyantoro S., and Daryono D., Identification of active faults in West Java, Indonesia, based on earthquake hypocenter determination, relocation, and focal mechanism analysis, Geoscience Letters, Vol. 5, No.31, pp.1-10.
[36] Muntafi Y. and Nojima N., Seismic Properties and Fractal Dimension of Subduction Zone in Java And Its Vicinity using Data From 1906 to 2020, International Journal of GEOMATE, Vol.21, ssue 85, 2021, pp.71-83.
[37] Cattin R., and Avouac J., Modeling of mountain building and the seismic cycle in the Himalaya of Nepal, J. Geophys. Res., Vol. 105, Issue B6, 2000, pp.389 – 407.
[38] Anggraini A., The 26 May 2006 Yogyakarta earthquake, aftershocks and interactions (Dissertation). Mathematisch-Naturwissenschaftlichen Fakultät der Universität Potsdam. Postdam, 2013, pp.1-107.
[39] Budiman R., Sahara D.P., and Nugraha A.D., Determining Source Model and Aftershocks of 2006 Yogyakarta Earthquake, Indonesia using Coulomb Stress Change, IOP Conference Series: Earth and Environmental Science, Vol. 318, 2019, pp.1-8.
[40] Clements B., Hall R., Smyth H.R., and Cottam M.A., Thrusting of a volcanic arc: a new structural model for Java. Petroleum Geoscience, Vol. 15, No. 2, .2009, pp.159–174.
[41] Sribudiyani, Muchsin N., Ryacudu R., Kunto T., Astono P., Prasetya I., Sapiie B., Asikin S., Harsolumakso A., and Yulianto I., The collision of east java microplate and its implication for hydrocarbon occurences in the east Java basin, Proceedings Indonesia Petroleum Association, 29th Annual Convention, 2003, pp.1-12.
[42] Huang L., and Liu C.-y., Three types of flower structures in a divergent-wrench fault zone, Journal of Geophysical Research: Solid Earth, Vol.22, Issue 12, 2017, pp.10478-10497.